Identification of the Pathway of Iontophoretic Drug Delivery: Light and Ultrastructural Studies Using Mercuric Chloride in Pigs

Nancy A. Monteiro-Riviere,[1,2] Alfred O. Inman,[1] and Jim E. Riviere[1]

Received March 2, 1993; accepted July 18, 1993

Although electrically assisted transdermal drug delivery has recently achieved a great deal of research attention, the precise anatomical pathway followed by these drugs through the stratum corneum has not been clearly defined. Pigs are an accepted model for studying iontophoretic drug delivery in humans. The purpose of this investigation was to visualize the pathway of ion transport by iontophoresing mercuric chloride. Weanling Yorkshire swine were dosed with 7.4% mercuric chloride in the positive electrode at a current density of 200 μAmp/cm^2 applied for 1 hr. Biopsies were immediately taken, exposed to 25% ammonium sulfide vapor to precipitate and localize the mercury, fixed, and processed for light and transmission electron microscopy. The presence of mercury, which appeared as a black precipitate, was confirmed using energy-dispersive X-ray microanalysis. Although some compound penetrated the skin through appendageal pathways, the electron micrographs clearly revealed that mercuric chloride traversed the intact stratum corneum via an intercellular route. Precipitate was also localized in the outer membrane of the mitochondria in the viable epidermal cells, dermal fibroblasts, and capillaries, demonstrating transdermal delivery and systemic exposure to the mercury. These findings have implications for iontophoretic drug delivery, since they allow visualization of the functional "pores" predicted by mathematical models.

KEY WORDS: pigs; iontophoresis; pathway; drug delivery; mercuric chloride; skin; light microscopy; electron microscopy.

INTRODUCTION

Electrically assisted transdermal drug delivery (e.g., iontophoresis, electroosmosis) has recently achieved a great deal of research attention. This type of delivery involves the transfer of ions or charged drugs through the skin in the presence of an electric current. Transdermal delivery of this kind permits administration of therapeutic compounds that would not normally penetrate the skin. However, the anatomical pathway through which a compound traverses the stratum corneum has not been precisely defined (Fig. 1). Studies using *in vitro* human abdominal skin suggest that the pathway a compound travels is by the intercellular route (1). Additional *in vitro* studies in hairless mouse skin assessing ion and current fluxes using a vibrating probe have implicated the appendageal pathways as the predominant route of electrically assisted drug delivery (2). Also, cathodic iontophoretic transport of a fluorescein dye in dermatomed human skin showed that transport can occur through a "pore" such as a hair follicle, a sweat duct, or an imperfection in the skin (3). Previous studies in our laboratory using *in vivo* and *in vitro* porcine skin demonstrated a pattern of morphological changes induced by lidocaine hydrochloride iontophoresis which suggest that epidermal alterations occur at focal areas and are only occasionally associated with hair follicles (4). Assuming these changes are related to the presence of transported drug, these findings suggest interfollicular transport may be important and should not be discounted. A knowledge of the actual pathway a drug follows during delivery is of obvious toxicological significance as well as offering support for competing mathematical models of pore transport. Pigs are an accepted model for the study of iontophoretic drug delivery in humans since their skin is morphologically and functionally similar (5,6). The sparce density of hair follicles in pig skin resembles that of human skin. Bronaugh *et al.* (5) have shown that hair density is 11 hair follicles/cm^2 in human and pig skin, while it is 289/cm^2 in rats, 658/cm^2 in mouse, and 75/cm^2 in hairless mouse. The use of hairy skin with a high density of follicles (e.g., rodents) may not be appropriate since the results would be heavily biased toward follicular transport due to the sheer density of hair follicles. Even the use of hairless animals could be misleading because rudimentary follicles are present though the shafts are lacking.

The pathway of ion transport was investigated by iontophoresing mercuric chloride as a test compound. The purpose of this investigation was (a) to search for evidence of an iontophoretic pathway, (b) to determine if this pathway follows an intracellular or intercellular route, and (c) to determine the extent or depth of the pathway.

MATERIALS AND METHODS

Female weanling Yorkshire pigs (n = 3) weighing 15–25 kg were sedated with an intramuscular injection of ketamine (10 mg/kg) and xylazine (4.0 mg/kg) and placed in a dorsal recumbent position. The hair was carefully trimmed with scissors from the caudolateral epigastric region of each pig. Iontophoretic electrodes, made of Porex and prepared as described previously (4), had either a 4.5- or a 3.0-cm^2 delivery area. The active electrode was saturated with a 7.4% (w/v) aqueous solution of mercuric chloride. The indifferent electrode was saturated with a 10% aqueous sodium chloride solution and placed caudal to the active electrode. Each electrode was positioned on the skin, covered with a piece of Parafilm (American Can Co., Greenwich, CT) to prevent evaporation, and secured with Elasticon tape (Johnson and Johnson, New Brunswick, NJ). The active electrode was connected by a standard alligator clip to the positive pole of a battery-powered constant-current generator (Model A360R, World Precision Instruments, Hamden, CT). The indifferent electrode was connected to the negative pole of the same generator unit. A Beckman 300 multimeter (Beckman Industrial Corp., San Diego, CA) was used to ensure a constant current of 900 μAmp (4.5-cm^2 electrode) or 600-μAmp (3.0-cm^2 electrode) and a subsequent current density

[1] Cutaneous Pharmacology and Toxicology Center, College of Veterinary Medicine, North Carolina State University, 4700 Hillsborough Street, Raleigh, North Carolina 27606.

[2] To whom correspondence should be addressed.

0724-8741/94/0200-0251$07.00/0

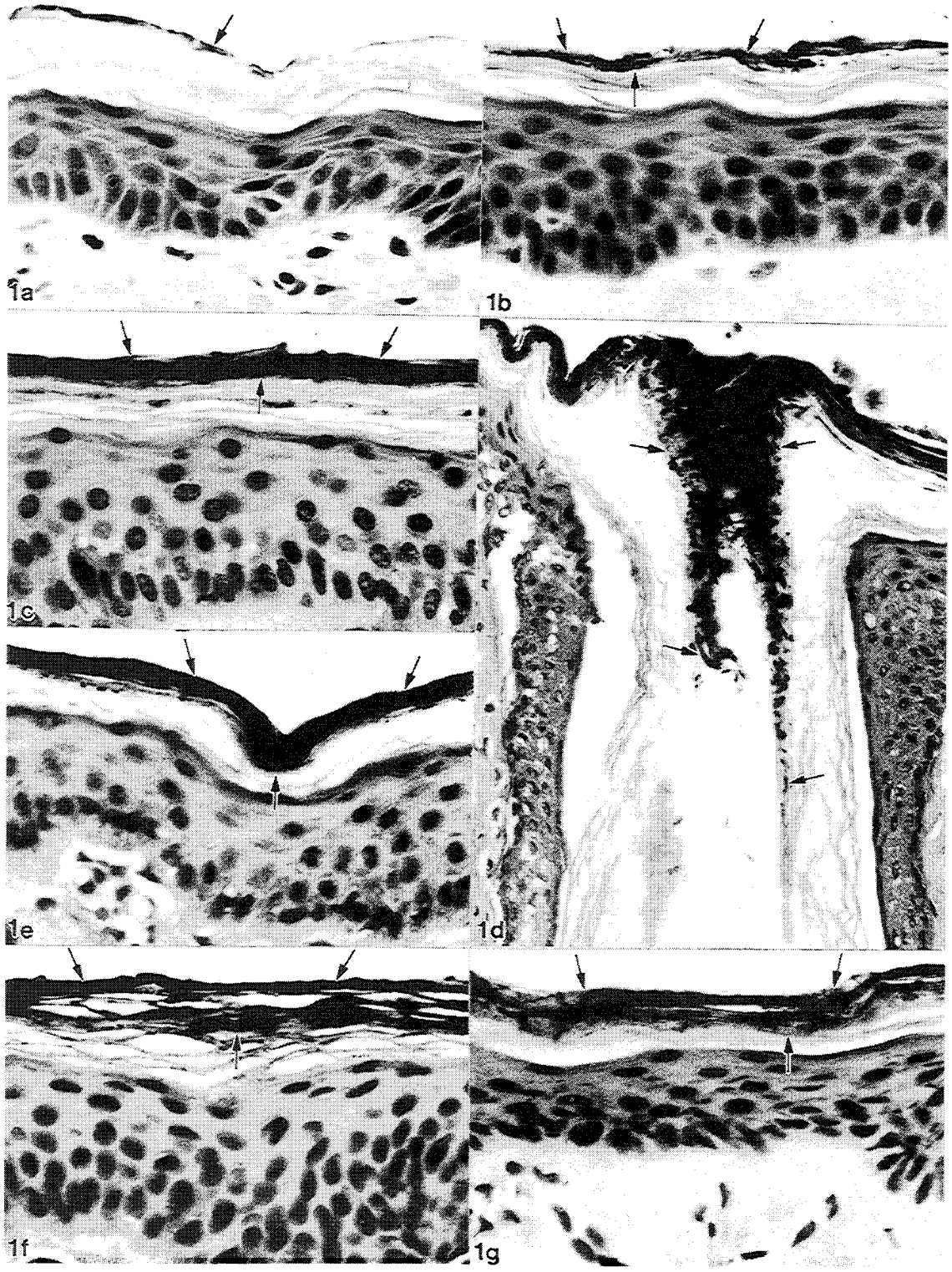

Fig. 1. (a) Light micrograph of mercuric sulfide, which appears as a focal granular black precipitate (arrow) on the surface of the stratum corneum (2 min of ammonium sulfide development). H&E. (b) Light micrograph of mercuric sulfide, which appears as a homogeneous black line (arrows) on the surface of the stratum corneum (10-min development). H&E. (c) Light micrograph of mercuric sulfide, appearing as a homogeneous dense black line (arrows) on the surface of the stratum corneum (15-min development). H&E. (d) Light micrograph of the precipitant (arrows) extending into the upper one-fourth of the hair follicle (15-min development). H&E. (e) Light micrograph of mercuric sulfide precipitant (arrows) uniformly distributed on the stratum corneum (30-min development). H&E. (f) Light micrograph of mercuric sulfide precipitant (arrows) uniformly distributed and penetrating through the stratum corneum layers (60-min development). H&E. (g) Light micrograph of mercuric sulfide precipitant (arrows) extending through 75% of the stratum corneum (90-min development). (a–d, f, g) H&E. 625× and (e) 335×.

of 200 μAmp/cm^2 for 1 hr. Pigs 1 and 2 were each iontophoresed at one site, while pig 3 was iontophoresed at two sites (left and right side). An additional pig was used to study passive delivery of mercuric chloride. Mercuric chloride was dosed directly onto the electrode until it became saturated and then placed on the caudolateral epigastric region without current for 1 hr. Following iontophoresis, the pigs were euthanatized with Beuthanasia-D (Schering-Plough, Kenliworth, NJ). The skin under each active electrode was dissected to the subcutaneous layer, rinsed 30 sec in phosphate-buffered saline, and blotted dry. The tissue sample was divided and exposed to the vapor of a 25% ammonium sulfide solution for varying times (0.5, 1.0, 1.5, 2.0, 5, 10, 15, 30, 45, 60, and 90 min) to form the immobile mercuric sulfide precipitant. In the passive delivery experiment, the skin was exposed to ammonium sulfide for 1 hr. Additional nondosed pig skin samples were developed in ammonium sulfide for 1 hr to serve as controls. All tissue samples were fixed in 2% paraformaldehyde and 2.5% glutaraldehyde in 0.2 *M* cacodylate buffer (pH 7.4) (light and transmission electron microscopy) or 4% formaldehyde and 1% glutaraldehyde in 0.2 *M* phosphate buffer (pH 7.3) (dispersive X-ray microanalysis) overnight at 4°C.

Samples for light microscopy (LM) were processed and infiltrated in a Tissue Tek VIP 1000 Processor (Miles Laboratories, Inc., Elkhart, IN) and embedded in a Tissue Tek embedding station (Miles Laboratories). Skin samples were cut at approximately 6 μm on a Reichert-Jung 820 rotary microtome, floated on a gelatin water bath at 37°C, and placed on glass slides. Sections were stained with hematoxylin and eosin (H&E) in an automatic tissue stainer (Histomatic Slide Stainer-Code on Series, Fisher Scientific), coverslipped with Permount (Fisher), and allowed to dry before evaluations were performed. Samples for routine transmission electron microscopy (TEM) were postfixed in 1% osmium tetroxide for 1 hr, dehydrated through a graded series of ethanol, cleared in acetone, infiltrated and embedded in Spurr's resin, then placed in flat embedding molds and polymerized at 70°C overnight. Sections 1 μm thick were stained with toluidine blue for orientation. Ultrathin sections (800–1000 Å) were cut with a diamond knife on a Reichert Ultracut E ultramicrotome and picked up on 75/300-mesh copper grids, and unstained sections photographed on a Philips 410 transmission electron microscope at an accelerating voltage of 80 kV.

The TEM tissue samples processed for energy-dispersive X-ray microanalysis followed the standard TEM protocol with the omission of the osmium tetroxide postfixation. Ultrathin sections were mounted on carbon-coated copper grids for analysis. Energy dispersive X-ray microanalysis was carried out on an ETEC autoscan scanning electron microscope (20 kV, 1.0 nA, 4000× magnification) interfaced to a Link System AN 10000 energy-dispersive X-ray microanalysis system (Link Analytical, Redwood, CA). The sample was tilted 30° toward the detector and analysis performed using a 50-sec acquisition time.

RESULTS

This experiment showed that the density of the mercuric sulfide precipitate was directly proportional to the ammonium sulfide vapor development time. Therefore, one must be cautious and aware that the duration of development as well as the method of microscopy utilized to visualize precipitate localization may affect the interpretive analysis.

LM

LM analyses of the 0.5-, 1.0-, 1.5-, 2.0-, 5-, and 10-min exposures to 25% ammonium sulfide showed little of the mercuric sulfide precipitant on the stratum corneum surface. Samples developed for 15, 30, 45, 60, and 90 min produced a significant amount of mercuric sulfide precipitant between the stratum corneum cell layers.

Samples stained with H&E depicted a consistent black granular banding pattern on the upper surface of the stratum corneum layers after the 10-min development. Exposure to ammonium sulfide for 0.5, 1.0, 1.5, and 2.0 min demonstrated a faint focal granular precipitate on the upper layers of the stratum corneum (Fig. 1a). This uneven distribution was present until the 10-min development, in which a very fine line was observed (Fig. 1b). The 15-min development showed uniform deposits on the surface of the stratum corneum layers (Fig. 1c) and in hair follicles (Fig. 1d). The precipitate, localized primarily in the upper portion of the hair follicle, extended to a depth of 94 μm, and therefore did not penetrate down the entire follicle. The 30-min development consisted of a dark uniform precipitate localized in the upper 25% of the stratum corneum which measured to a depth of 5.6 μm (Fig. 1e). In the 60-min development, the uniform precipitate penetrated 50% (8.3 μm) of the stratum corneum (Fig. 1f). At the 90-min development, the precipitate penetrated 75% (11.12 μm) into the stratum corneum layers (Fig. 1g). Although the mercuric sulfide precipitate increased with exposure to ammonium sulfide, none was noted by LM in the lower 25% of the stratum corneum or in the epidermis. Passive delivery of mercuric chloride for 1 hr, followed by a 1-hr development by ammonium sulfide showed the precipitate to penetrate uniformly through the upper 25% of the stratum corneum. Additional nondosed pig skin control samples developed in ammonium sulfide for 1 hr showed no background precipitate.

TEM

TEM clearly revealed the exact anatomical pathway of mercuric chloride transdermal iontophoresis. The 0.5-, 1.0-, 1.5-, 2.0-, and 5-min development showed the precipitate to aggregate primarily on the surface of the stratum corneum, occasionally penetrating one stratum corneum cell layer. Following a 10-min development, the precipitate penetrated one or two stratum corneum layers (Fig. 2a). After a 15-min development (Fig. 2b), the most superficial layers of the stratum corneum contained a fine granular deposit intracellularly, while in the lower layers the precipitate was found as far down as 15 cell layers and localized within the intercellular spaces. Also, a few granules of the precipitate were present within the cells of the stratum granulosum, stratum spinosum, and stratum basale. The precipitate was localized to the outer mitochondrial membrane of the mitochondria in these viable cells (Fig. 2c). In some instances, granules were present in the superficial capillaries of the papillary dermis and in the fibroblast processes (Fig. 2c). This finding con-

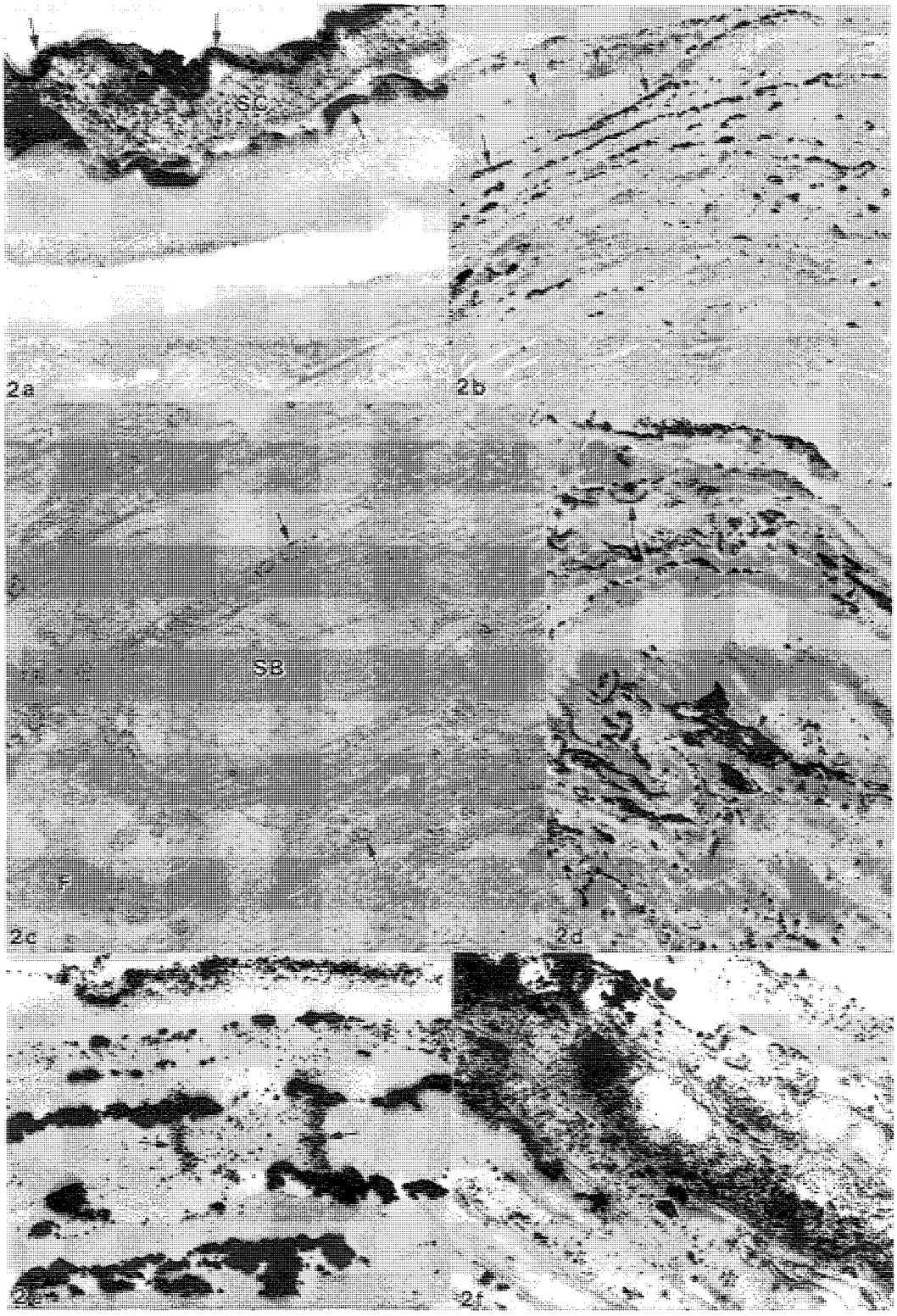

Fig. 2. (a) Transmission electron micrograph showing the black mercuric sulfide precipitate (arrows) extending through only the upper layer of the stratum corneum (SC) (10-min development). (b) Transmission electron micrograph depicting mercuric sulfide deposits that are intracellular (arrowheads) in the most superficial stratum corneum layers, while farther down the stratum corneum layers the deposit is intercellular (arrows) (15-min development). (c) Electron micrograph depicting precipitate granules in the outer mitochondrial membrane (arrows) of the stratum basale (SB) cells of the epidermis. Note the additional black granules in the mitochondria of the fibroblast (F) (15-min development). (d) Electron micrograph depicting intercellular localization of mercuric sulfide (arrowheads) in the stratum corneum layers. Note the crescent-shaped granular deposits (arrows) (30-min development). (e) Higher magnification depicting mercuric chloride precipitate located intercellularly. In focal regions, the precipitant aggregates with fine granules funneling intracellular (arrows) (60-min development). (f) Mercuric sulfide is pronounced and overdeveloped, with large disorganized deposits of the precipitant (arrow) (90-min development). (a) 79,950×, (b) 6985×, (c) 9720×, (d) 6200×, (e) 36,700×, and (f) 46,350×; reduced to 90% for reproduction.

firms the high probability of transdermal iontophoretic delivery. After a 30-min development, the precipitate extended down to 21 cell layers and was located between the individual stratum corneum cells. Also, crescent-shaped granular deposits were occasionally present within the upper layers of the stratum corneum (Fig. 2d). A higher magnification precisely revealed that this precipitate was located intercellularly. After a 60-min development to ammonium sulfide, the precipitate extended down to 15 cell layers. In focal regions, the precipitant aggregated intercellularly, with fine granules funneling intracellularly. However, the predominant route was intercellular (Fig. 2e). After 90 min of development, the depth of penetration did not exceed that of a 60-min development. The accumulation of these deposits was larger and more disorganized, within and between the stratum corneum cell layers (Fig. 2f).

Passive delivery of mercuric chloride revealed that the granular precipitate penetrated to a depth of 12 corneum cell layers. No precipitate was present in the viable epidermis or dermis. The black precipitate was primarily observed to be intracellular. Occasionally, fine intercellular granules of a different density were noted. Nondosed pig skin developed for 1 hr with ammonium sulfide showed no black reaction product.

Energy-dispersive X-ray microanalysis was performed to validate the identity of this precipitate. The X-ray emission spectrum clearly showed that the intercellular precipitate was indeed mercury (Fig. 3a). The presence of copper, iron, and silicon peaks represent emissions from the carbon-coated grids and background noise from the scope. The spectrum from an adjacent precipitant-free area demonstrated only background noise, and no mercury peaks (Fig. 3b).

DISCUSSION

These studies unequivocally show that iontophoresis of mercuric chloride occurs via an intercellular pathway in *in vivo* porcine skin. This is in agreement with *in vitro* human skin studies (1). Also, exposure to ammonium sulfide vapors for a short time period was not adequate to form the immobile mercuric sulfide precipitant. At least 15 min of development by ammonium sulfide was necessary to produce sufficient precipitate for localization. Exceedingly long exposure times may decrease the resolution of localizing precipitate to subcellular structures. It must be stressed that this technique of mercury precipitation to localize the pathway of transdermal delivery does not measure active flux of the absorbed ion; rather it locates only precipitated mercury which has remained after 60 min of iontophoretic administration. However, it is axiomatic that the precipitate reflects mercury which has traversed this pathway. The localization of this precipitate in deep epidermal and dermal regions by TEM after iontophoresis, but not by passive delivery, confirms the potential for transdermal delivery by iontophoresis. The results of passive mercury delivery are essentially identical to those reported previously in human skin (7) and in the nude mouse (8).

The pathway of mercuric chloride initially was intracellular through the first few layers of the stratum corneum, but as the path progressed through the stratum corneum it became primarily intercellular. Mercuric chloride may have a binding affinity to cell membranes. The most superficial stratum corneum cells, called stratum disjunctum, are able to desquamate quite easily due to the enzymatic degradation of the desmosome junctional complex. This may explain the intracellular location of precipitant at these very superficial sites. This intracellular localization of mercuric chloride in the upper few layers of the stratum corneum was also demonstrated by passive delivery in human skin *in vitro*, in human plantar callus, and with iontophoresis through human abdominal skin (1,7). Studies in neonatal mouse and human

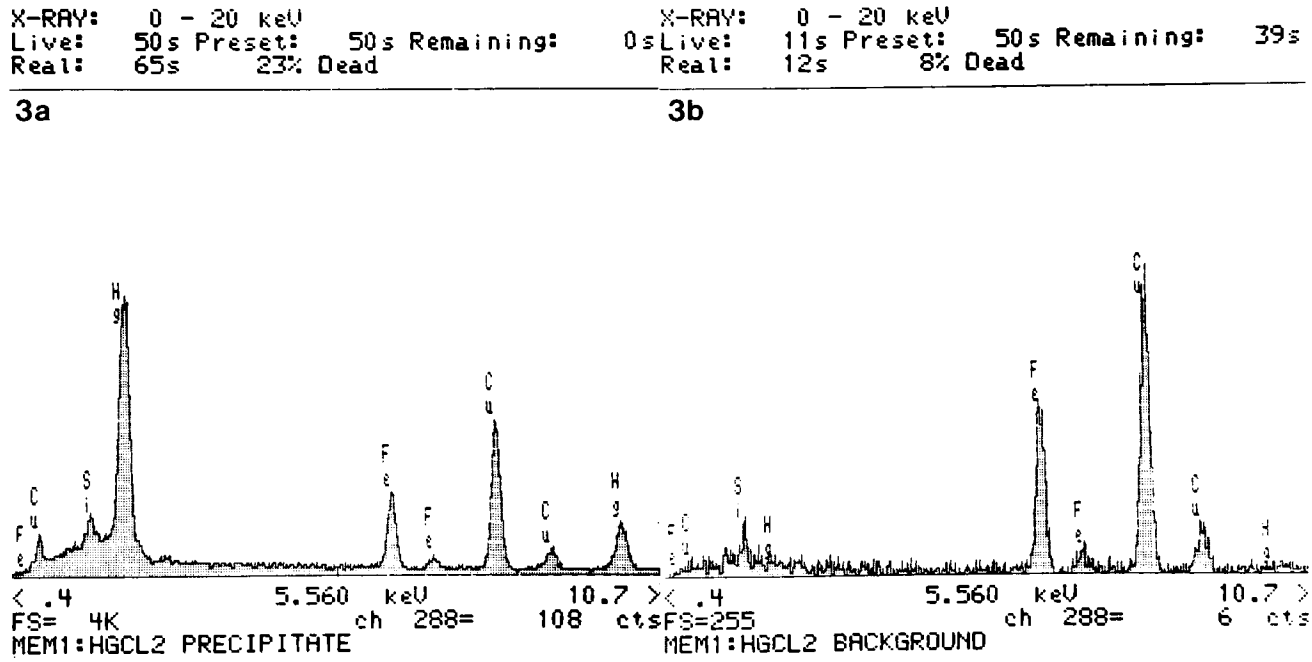

Fig. 3. (a) An X-ray emission spectrum validating mercury (Hg) as the primary intercellular precipitant. (b) An X-ray emission spectrum from an adjacent precipitant-free area showing background noise with no mercury peaks.

stratum corneum immersed in *n*-butanol and precipitated with osmium vapor also demonstrated that flocculent osmium deposits of varying densities were present within the corneocytes as well as within the intercellular space (9).

Other studies have shown that the stratum corneum consists of two functionally different components. The upper few layers of loosely attached cells are considered to be functionally desquamated, while the deeper stratum corneum cells are highly resistant to different forms of mechanical insult (10,11). It is the most superficial layers of the stratum corneum that can be easily sloughed off due to the enzymatic degradation of the desmosomes and are more subject to picking up compounds intracellularly. This was demonstrated by this study, where the upper layers of the stratum corneum contained mercuric chloride. In addition, desmosomes and tight junctions are the only epithelial cellular adhesions found in the stratum corneum layers. Degradation of the desmosomes may take place at the desmosomal core, which is known to contain two types of glycoproteins (desmocollins and desmogleins). These may break down, thereby disrupting the cellular adhesion and allowing the penetration of mercuric chloride. The crescent-shaped granular deposits seen in the stratum corneum layers may reflect this pathway. These arc-shaped fronts were also seen after 2 hr *in vitro* in human skin stratum corneum using a two-compartment diffusion cell (7). Mercury accumulation at these stratum corneum sites relative to other regions studied implies that this level of the stratum corneum may be a primary resistance barrier to iontophoretic delivery.

The intercellular pathway for delivery of mercuric chloride by iontophoreis may also provide an anatomical basis for interpreting potential size restrictions on defining the putative "pores" in mathematical models that assume an intercellular pathway. The maximal diameter would be the width of the intercellular space, and not that of a hair follicle shaft or sweat duct. Note that even with follicular transport, the final pathway is still intercellular between hair follicle epidermal cells. Additionally, the actual surface area available for transport in a hair follicle reflects the area of the invagination, and not just the opening on the surface. In all probability, the diameter of the intercellular space would be an exaggerated upper limit since ion passage would occur between lipid sheaths which comprise the intercellular space (12–14). Additional anatomical studies need to be performed to localize such a pathway within the intercellular lipid matrix. As in passive delivery of lipid soluble drugs, the intercellular pathway suggests significant tortuosity, which increases the path length nonlinearly from that estimated by stratum corneum and epidermal size and thickness alone.

In conclusion, these studies support the hypothesis that the predominant pathway for transdermal drug delivery in both passive and active systems is the intercellular route (1,7). This finding has implications in interpreting mathematical models of iontophoretic transport which postulate pores as being the route of entry.

ACKNOWLEDGMENTS

This study was partially supported by the Becton Dickinson Research Center. A portion of this manuscript was presented at the Sixth Annual Meeting of the American Association of Pharmaceutical Scientists, Washington, DC, November 17–21, 1991. The authors would like to thank Ms. Elise Cash for histological assistance and Dr. Peter Ingram of the Research Triangle Institute, Research Triangle Park, NC, for his assistance with X-ray microanalysis.

REFERENCES

1. H. E. Bodde, F. H. N. de Haan, L. Kornet, W. H. M. Craanevan Hinsberg, and M. A. Salomons. Transdermal iontophoresis of mercuric chloride *in vitro:* electron microscopic visualization of pathways. *Proc. Int. Symp. Control. Rel. Bioact. Mater.* 18:301–302 (1991).
2. C. Cullander and R. H. Guy. Sites of iontophoretic current flow into the skin: Identification and characterization with the vibrating probe electrode. *J. Invest. Dermatol.* 97:55–64 (1991).
3. R. R. Burnette and B. Ongpipattanakul. Characterization of the pore transport properties and tissue alteration of excised human skin during iontophoresis. *J. Pharm. Sci.* 77:132–137 (1988).
4. N. A. Monteiro-Riviere. Altered epidermal morphology secondary to lidocaine iontophoreis: *in vivo* and *in vitro* studies in porcine skin. *Fundam. Appl. Toxicol.* 15:174–185 (1990).
5. R. L. Bronaugh, R. F. Stewart, and E. R. Congdon. Methods for in vitro percutaneous absorption studies. II. Animal models for human skin. *Toxicol. Appl. Pharmacol.* 62:481–488 (1982).
6. N. A. Monteiro-Riviere. Comparative anatomy, physiology and biochemistry of mammalian skin. In D. W. Hobson (ed.), *Dermal and Ocular Toxicology: Fundamentals and Methods,* CRC Press, Boca Raton, FL, 1991, pp. 3–71.
7. H. E. Bodde, I. van den Brink, H. K. Koerten, and F. H. N. J. de Haan. Visualization of *in vitro* percutaneous penetration of mercuric chloride: Transport through intercellular space versus cellular uptake through desmosomes. *Control. Release* 15:227–236 (1991).
8. H. H. Sharata and R. R. Burnette. Effect of dipolar aprotic permeability enhancers on the basal stratum corneum. *J. Pharm. Sci.* 77:27–32 (1988).
9. M. K. Nemanic and P. M. Elias. A novel cytochemical technique for visualization of permeability pathways in mammalian stratum corneum. *J. Histochem. Cytochem.* 28:573–578 (1980).
10. A. Lundstrom and T. Egelrud. Cell shedding from human plantar skin in vitro: Evidence of its dependence on endogenous proteolysis. *J. Invest. Dermatol.* 91:340–343 (1988).
11. A. Lundstrom and T. Egelrud. Evidence that cell shedding from plantar stratum corneum in vitro involves endogenous proteolysis of the desmosomal protein desmoglein I. *J. Invest. Dermatol.* 94:216–220 (1990).
12. D. C. Swartzendruber, P. W. Wertz, D. J. Kitko, K. C. Madison, and D. T. Downing. Molecular models of the intercellular lipid lamellae in mammalian stratum corneum. *J. Invest. Dermatol.* 92:251–257 (1989).
13. K. C. Madison, D. C. Swartzendruber, P. W. Wertz, and D. T. Downing. Presence of intact intercellular lipid lamellae in the stratum corneum. *J. Invest. Dermatol.* 88:714–718 (1987).
14. G. K. Menon, K. R. Feingold, and P. M. Elias. Lamellar body secretory response to barrier disruption. *J. Invest. Dermatol.* 98:279–289 (1992).